Journal of Renewable Materials

Tech Science Press

DOI: 10.32604/jrm.2023.044310

ARTICLE

Carrageenan Fiber Prepared by a New Process Route of Ba^{2+} Ion Pre-Crosslinking in the Spinning Solution

Liting Jia[1], Xiao Han[1], Cuixia Qiao[2], Gang Zhao[2], Yanzhi Xia[1] and Zhixin Xue[1,*]

[1]School of Chemistry and Chemical Engineering, State Key Laboratory of Bio-Fibers and Eco-Textiles, Marine Fiber New Material Institute, Qingdao University, Qingdao, 266071, China

[2]Department of Traditional Chinese Medicine, The Affiliated Hospital of Qingdao University, Qingdao, 266000, China

[*]Corresponding Author: Zhixin Xue. Email: xuezhixin@qdu.edu.cn

Received: 27 July 2023 Accepted: 17 October 2023 Published: 11 April 2024

ABSTRACT

Ba^{2+} pre-crosslinked carrageenan fiber (Ba/CAF) was prepared by adding a small amount of Ba^{2+} to the carrageenan (CA) solution as the spinning solution. Ba/CAF-n/A, Ba/CAF-n/B and Ba/CAF-n/C were prepared with ethanol solution (combine A), high concentration $BaCl_2$ solution (combine B) and low concentration $BaCl_2$ solution (combine C), as coagulation bath and stretch bath, respectively. The combination of coagulation bath and stretch bath suitable for Ba^{2+} pre-crosslinking wet spinning was screened. The results showed that Ba^{2+} can induce the birefringence of the CA molecular chain, and the Ba^{2+} pre-crosslinking effect is the best when the CA mass fraction is 8.0 wt%. From the perspective of production safety, fiber performance and spinning cost, the coagulation bath of 3.5 wt% $BaCl_2$ solution and stretch bath of 1.7 wt% $BaCl_2$ solution, that is, combination C with low concentration $BaCl_2$ solution, is the best choice. Ba/CAF-8.0/C was obtained under the best conditions. The linear intensity, water absorption and flame retardancy study showed that the breaking strength of Ba/CAF-8.0/C is as high as 1.61 cN/dtex, the water absorption was 649.2% and 574.3%, in deionized water and normal saline, respectively, and the LOI value reached 32.

KEYWORDS

Carrageenan fiber; Ba^{2+} ion; pre-crosslinking; wet spinning; flame retardancy

1 Introduction

Carrageenan (CA) is a hydrophilic polysaccharide extracted from red algae. It is composed of sulfated or non-sulfated galactose and 3,6-dehydrodylated lactone galactose by alternate linking of the α-1,3- glycosidic bonds with the β-1,4 glycosidic bonds [1]. Carrageenan is usually used as thickener, gelling agent, suspension agent and emulsifier in the food, medical and cosmetics industry because of its water solubility, gelation ability, biocompatibility, environmental friendliness and renewability [2]. The latest research shows that carrageenan also has the potential for application in the textile industry. Commonly, there are three kinds of carrageenan, i.e., κ-CA, ι-CA and λ-CA commercially available [3,4].

The main difference between the three types of carrageenan is the number and location of the sulfate group in the repeating six-membered chain segment. The contents of sulfate groups of the three types of carrageenan were 18%–25%, 25%–34% and 30%–40%, respectively. The number and location of sulfate

groups are the main factors affecting their performance differences [5,6]. The higher the content of sulfate, the lower the dissolution temperature and the weaker the gelation ability. On the contrary, the lower the content of sulfate, the higher the dissolution temperature and the stronger the gelation ability. It is generally believed that the content of sulfate is directly proportional to the ease of gel formation [4]. Therefore, considering the type characteristics of carrageenan comprehensively, ι-CA is used when preparing carrageenan fiber. It is not specified in this article that the carrageenan used refers to ι-CA.

Normally, carrageenan dissolves in hot water and becomes a gel at low temperatures. We have invented a method of dissolving carrageenan in NaOH solution to solve the problem of wet spinning at room temperature [7]. In recent years, a variety of metal ions have involved in the cross-linking between polysaccharide polymers to prepare seaweed fibers, which can be applied to improve flame retardancy and breaking strength properties [8–10]. In the traditional wet spinning process of carrageenan fiber, the binding between metal ions and carrageenan molecules occurs in the coagulation and stretch baths, but the short contact time during the spinning process is difficult to ensure complete binding of carrageenan molecules and metal ions. In addition, as the spinning process progresses, the concentration of metal ions in coagulation and stretch baths gradually decreases, and the change of concentration may lead to differences in the same batch of fibers.

To solve this problem, Min Dong has developed a method of wet spinning by adding Ba^{2+} to the spinning solution, followed by using recyclable alcohol in coagulation and stretch baths [11]. The tensile strength of carrageenan fiber obtained by this method is 1.63 cN/dtex, which is twice that of the traditional process. Although the strength of the so-prepared fiber has been significantly improved, there are still some problems in actually production [12]. Such as, high-concentration ethanol is flammable and explosive, and there are great security risks in industrial production; the concentration of metal ion remaining in the coagulation and stretch baths during the spinning process also decreased; the recovery of ethanol increases the cost of fiber spinning [13].

Based on the above reasons, in the present work, Ba^{2+} pre-crosslinking method was adopted to prepare spinning solution, and three different combinations of coagulation bath and stretch bath were selected to prepare Ba^{2+} pre-crosslinked carrageenan fiber by wet spinning process to seek a safer and more efficient combination to improve the mechanical properties of the fiber.

2 Experimental

2.1 Materials

ι-Carrageenan powder was purchased from Shi Shi Globe Agar Industries Co., Ltd. (Quanzhou, China), and used without further treatment. All other reagents used in the experiment are analytical grade reagents.

2.2 Preparation of Ba/CA and Ba/CAF

2.2.1 Preparation of Carrageenan Spinning Solution Contained Ba^{2+} Ions-Ba/CA

Carrageenan solution with different concentration of 7.0 wt%, 7.5 wt%, 8.0 wt% and 8.5 wt% contained 4.6 mM $BaCl_2$ and 8% NaOH was obtained by dissolving proper carrageenan, $BaCl_2$ and NaOH powder in distilled water, and heated in water bath at 85°C under stirring. The so-prepared solutions were used as spinning solution, which were labeled as Ba/CA-7.0, Ba/CA-7.5, Ba/CA-8.0 and Ba/CA-8.5.

Then, let those spinning solution stand and defoamed for about 12 h before used.

2.2.2 Preparation of Carrageenan Fiber with Ba^{2+} Pre-Crosslinked in Spinning Solution-Ba/CAF

The wet spinning process for the preparation of Ba/CAF was shown in Fig. 1. The different fibers were produced from different spinning solution (I), went through coagulation and stretch baths (II), and washed with 50% ethanol and 95% ethanol (III), and then dried at room temperature (IV). In the spinning process, the

speed of the metering pump is set to 30 r/min, the drawing ratio is set to 1:1.2, the specification of the spinneret is 0.08 mm × 60 mm, and the pre-loading pressure is 0.2 MPa.

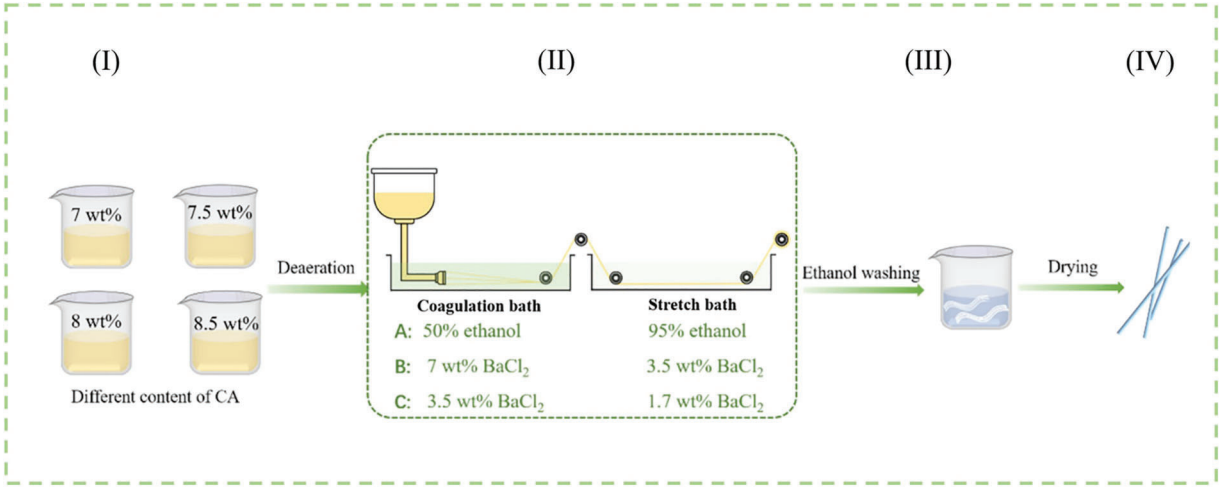

Figure 1: Ba^{2+} pre-crosslinked wet spinning process

There were three combinations A, B and C set in different coagulation and stretch baths. Of which,

A, 50% ethanol solution as coagulation bath, 95% ethanol solution as stretch bath;

B, 7 wt% $BaCl_2$ solution as coagulation bath, 3.5 wt% $BaCl_2$ solution as stretch bath;

C, 3.5 wt% $BaCl_2$ solution as coagulation bath, 1.7 wt% $BaCl_2$ solution as stretch bath.

The fibers so-prepared were denoted as Ba/CAF-n/A, Ba/CAF-n/B, Ba/CAF-n/C according to the combination of coagulation and stretch baths, and n was the concentration of carrageenan in the spinning solution.

2.3 Characterizations of Ba/CA

2.3.1 Testing of Viscosity

The viscosity of the Ba/CA at 25°C was measured by a rotary viscometer (MRV) (BROOKFIELD DV-II+ Pro, USA). After turning on the machine, adjust the position of the rotary viscometer so that it is in the horizontal state. The rotor model used for the test is 64, and the speed is set to 6 rpm. Record after the viscosity indicator of the sample was stable.

2.3.2 Testing of Polarizing Light Microscopy

The pre-cross-linking structure of Ba/CA was observed by polarization light microscope (PLM) (DM4P, Leica, German). Transfer the micro spinning solution to a glass slide with an eyedropper and press one side of the cover glass against the sample droplet so that the surface of the droplet is completely covered. The samples were observed and photographed in an orthogonal arrangement.

2.3.3 Testing of Dynamic Light Scattering

The particle size distribution of Ba/CA was measured by laser particle size analyzer (Nano ZSE, England). The test temperature was set at 25°C, and the dynamic light scattering (DLS) angle θ was 173°. The experimental data were analyzed by Zetasizer Software (Mastersizer 3000, England).

2.4 Characterizations of Ba/CAF

2.4.1 Testing of Scanning Electron Microscopy

The morphology of the cross and surface sections of the Ba/CAF was observed by scanning electron microscopy (SEM) (Quanta 250 FEG, USA). All samples were treated with vacuum gold injection after labeling, and the surface and cross section morphology were tested at an accelerated voltage of 10 kV.

2.4.2 Testing of X-Ray Electronic Differential System

The elemental content of Ba/CAF was determined by X-ray electronic differential system (EDS) (Quanta 250 FEG, USA), Mapping analysis can obtain the distribution of selected elements in the microregion of the sample surface, and the acceleration voltage is set to 10 kV.

2.4.3 Testing of Fourier Transform Infrared Spectroscopy

The main functional groups of Ba/CAF were determined by infrared spectroscopy (FTIR) (Nicolet iS10, USA). During the test, the scan wavenumber range was set to 500–4000 cm^{-1}, and the resolution was set to 4 cm^{-1}. The total number of scans was 32.

2.4.4 Testing of Mechanical Properties

The mechanical properties of Ba/CAF were tested by automatic single fiber tester (Favimat-airobot, Germany). Test conditions: temperature 20 ± 5°C, humidity 30% R.H., standard distance 5 mm, test speed 10 mm/min, fiber length 10 cm, 20 samples, took the average.

2.4.5 Testing of Water Absorption

After drying to constant weight, the Ba/CAF were immersed in deionized water and normal saline (0.9% NaCl solution), respectively. After 15 min, they were taken out and dried naturally, and then weighed again. The mass (g) of the fibers before absorbing water was m_0, and the mass (g) of the fibers after absorbing water and drying was m. The Water absorption degree of the fiber can be calculated according to formula (1):

$$\text{Water absorption degree} = \frac{m - m_0}{m_0} \times 100\% \quad (1)$$

2.4.6 Testing of the Limiting Oxygen Index

The limiting oxygen index (LOI) value of Ba/CAF were determined by Hc-2 instrument (Beijing Innovation Instrument Equipment Co., Ltd., China). Weigh the 3 g Ba/CAF, press it into a 100 mm × 30 mm × 2 mm long strip sample with a hot press, and test it by the limit oxygen index instrument according to the international standard ASTMD2863.

3 Results and Discussion

3.1 Properties of Ba/CA

According to related literature [12], the preparation time of the spinning solution with uniform distribution and good fluidity at room temperature is about 2.5 h with the traditional method, while the method in this experiment only takes 1 h, because the introduction of Ba^{2+} performed at higher temperature accelerates the dissolution of the ι-CA powder.

Normally, the spinnability of a polymer solution depends on its viscoelasticity. The orthogonal experiment results in relevant literature have confirmed that the CA concentration in spinning solution is the key factor for fiber formation. When the concentration is lower than 7.0 wt%, it cannot be wet-spun into fiber, and only dispersed flocculent is produced in coagulation bath. When the concentration is higher than 9.0 wt%, the spinning liquid flows poorly at room temperature, and it is difficult to extrude from the spinneret. In this experiment, four concentrations of spinning solution were set, including

7.0 wt%, 7.5 wt%, 8.0 wt% and 8.5 wt%, and the viscosity of spinning solution was increased by Ba^{2+} pre-crosslinking.

The viscosity of BA/CA with different carrageenan concentrations at 25°C was shown in Fig. 2. It can be seen from Fig. 2 that the viscosity of the spinning solution was positively correlated with the concentration of CA at 25°C. Among them, the lowest viscosity is Ba/CA-7.0, which is only 27683 mPa·s; the viscosity of Ba/CA-7.5 and Ba/CA-8.0 are 29051 mPa·s and 32193 mPa·s, respectively; the highest viscosity is Ba/CA-8.5, which is 35632 mPa·s. With the increase of CA concentration, the interaction of hydrogen bonds between CA molecular chains and the interaction of Ba^{2+} with sulfate groups in CA molecules were enhanced, and the degree of entanglement between polymer chains increases, resulting in an increase in viscosity.

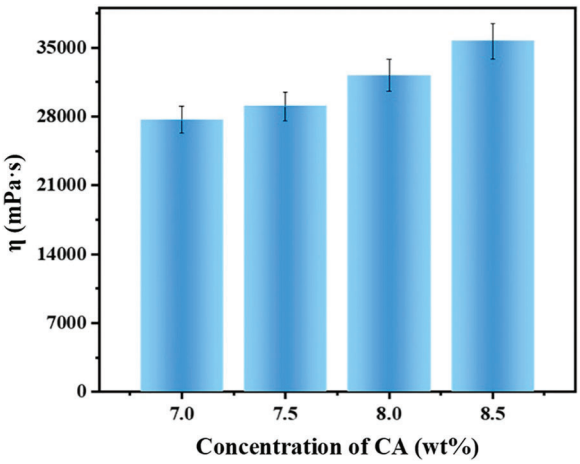

Figure 2: Viscosity of Ba/CA with different carrageenan concentrations at 25°C

After the introduction of Ba^{2+}, bright fine needles appeared in the spinning solution under PLM orthogonal alignment. The principle of PLM testing the crystal structure of substances is: If the subject under test contains isotropic substances, the linearly polarized light will not change the direction of vibration, and the linearly polarized light emitted from the polarizer cannot pass through the polarization analyzer, so the field of view remains dark [14]; If the subject contains anisotropic material, part of the linearly polarized light generated after birefringence can pass through the polarizer, and bright phenomena can be observed in the field of view. When light passes through different kinds of birefringence, the vibration direction of linearly polarized light changes, resulting in different bright phenomena [15].

It has been confirmed in relevant literature that the addition of Ba^{2+} will affect the orientation of CA molecular chains, and the experimental results show that Ba^{2+} changes its orientation by forming anisotropic birefringent. By comparison, it can be found that in Ba/CA-7.0 (Fig. 3a) and Ba/CA-7.5 (Fig. 3b), the birefringent shape is not clear, which indicates that the distribution of CA molecular chains is not completely uniform. In contrast, in Ba/CA-8.0 (Fig. 3c), the bright phenomenon is more obvious, the birefringent has a clear outline and obvious shape, and the arrangement of CA molecular chains is the most regular [12]. However, in Ba/CA-8.5 (Fig. 3d), the birefringent is no longer a single fine needle shape but branches, indicating that the distribution uniformity of CA molecular chains is reduced at this time, which is also consistent with the test results of particle size distribution in the following paper (Fig. 4).

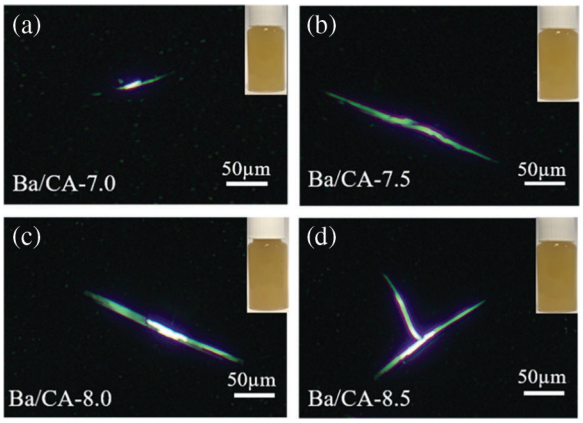

Figure 3: PLM image of Ba/CA with different carrageenan concentrations in orthogonal correction (Ba/CA photo in illustration)

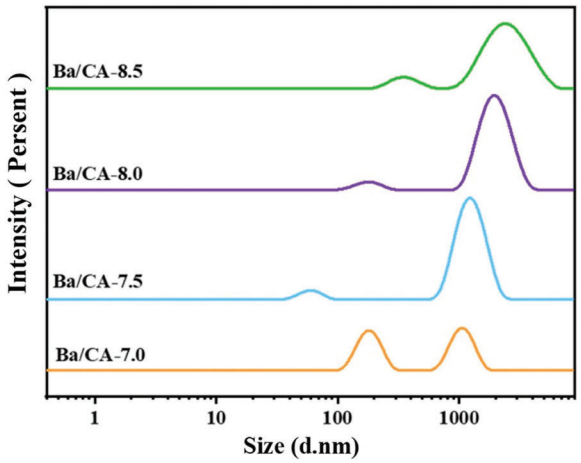

Figure 4: Particle size distribution of Ba/CA with different carrageenan concentrations at 25°C

The particle size distribution of the spinning solution (Fig. 4) also showed a similar pattern to the PLM observed above. Ba/CA-7.0 showed two similar peaks, accounting for 57.9% at 183.1 nm and 42.1% at 1071 nm. The mean value of hydrodynamic diameter (Z-Ave) was 702.8 nm, and the particle dispersion index (PDI) value was 0.620, indicating some difference in particle diameter in solution. In Ba/CA-7.5, the first peak at 58.8 nm accounted for 9.9%, the second peak at 1280 nm accounted for 90.1%, the Z-Ave was 1250 nm, and the PDI value was 0.609. The solution distribution was narrow and the second peak was dominant, indicating that the particle diameter began to converge at this time. In Ba/CA-8.0, the peak value at 164.1 nm accounted for only 6.2%, and the peak value at 1990 nm was as high as 93.8%, the Z-Ave was 1475 nm, and the PDI value was 0.614, indicating that the particle distribution of the spinning solution was relatively uniform and the particle diameter was basically the same at this time. However, in Ba/CA-8.5, the peak value at 179.9 nm accounted for 6.3%, the peak value at 2032 nm accounted for 93.7%, the Z-Ave was 1499 nm, and the PDI value was 0.810. At this time, the particle size distribution in the spinning solution was relatively wide, the particle size decreased and the distribution uniformity decreased.

3.2 Properties of Ba/CAF

According to the performance test results of the spinning solution, Ba/CA-8.0 has a suitable viscosity and uniform solution distribution, so Ba/CA-8.0 was selected for further spinning experiments. Fig. 5 shows the optical photograph (Figs. $5a_1$–$5c_1$), scan electron microscopic image (Figs. $5a_2$, $5b_2$, $5c_3$) and EDS (energy dispersive spectrometer) mapping (Figs. $5a_3$–$5c_3$) of Ba/CA-8.0s-Ba/CA-8.0/A, Ba/CA-8.0/B, Ba/CA-8.0/C.

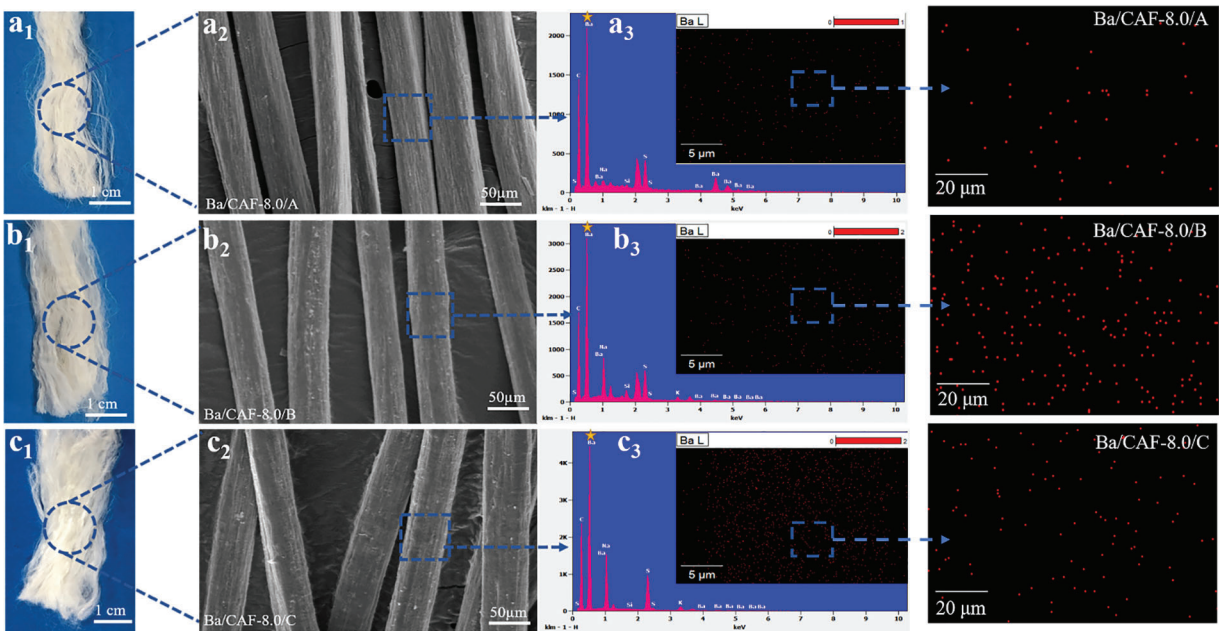

Figure 5: SEM and Elemental content analysis of Ba/CAF-8.0. (a) Ba/CAF-8.0/A, (b) Ba/CAF-8.0/B, (c) Ba/CAF-8.0/C a_1, b_1, c_1 optical photograph, a_2, b_2, c_2 SEM image, a_3, b_3, c_3 EDS

The surface morphology of the Ba/CAF-8.0s was observed by SEM. The comparative observation shows that the surface morphology of the fibers is closely related to the choice of the coagulation bath. Ba/CAF-8.0/A prepared by combination A (Figs. $5a_1$, $5a_2$) has a soft hand feel, smooth surface, uniform in fiber size with no obvious fiber adhesion. There is basically no fine granular attachment on the surface, but there are dense longitudinal stripes, which is caused by the dehydration of the primary fibers after ethanol treatment. Ba/CAF-8.0/B prepared by combination B (Figs. $5b_1$, $5b_2$) has the roughest surface, with a large number of fine granular attachment, which is the solidify substance formed by the combination of Ba^{2+} and the sulfate group in CA molecules in the coagulation bath. Due to the high concentration of $BaCl_2$ solution providing a large amount of Ba^{2+}, the surface solidify speed of the fiber is too fast. Metal ions could not enter the interior of the fiber, which resulted in uneven structure of the fiber, and a large amount of solidified material accumulated on the surface [16,17].

EDS test results also confirmed this conclusion. The Ba/CAF-8.0/C prepared by combination C (Figs. $5c_1$, $5c_2$) has a soft and fluffy feel, smooth surface and good splitting effect, less fine granular adhesion on the surface and sparse longitudinal stripes [18]. This is because the low concentration of Ba^{2+} is uniformly combined with the sulfate group in CA molecules in the coagulation bath, which makes the internal structure of the fiber dense and compact.

The distribution of Ba element on the fiber surface can be characterized by EDS, and the combined situation can also be analyzed by Mapping image, which provides a basis for the analysis of fiber

formation mechanism below [19]. The distribution of C, O, S and Ba on the Ba/CAF-8.0/A, Ba/CAF-8.0/B and Ba/CAF-8.0/C surfaces was characterized. The four elements were evenly distributed on the Ba/CAF-8.0/A surface (Fig. 5a$_3$). The C, O and S elements were dense, while the Ba elements were sparse. The characteristic peak of Ba indicates that the Ba element on the fiber surface is low, which is because the Ba element source in Ba/CAF-8.0/A is only the small amount of $BaCl_2$ added during pre-crosslinking, and the uniform distribution of Ba element indicates that Ba^{2+} can be uniformly combined with the sulfate group of CA molecules during pre-crosslinking.

EDS test results of Ba/CAF-8.0/B (Fig. 5b$_3$) and Ba/CAF-8.0/C (Fig. 5c$_3$) showed that the four elements were uniformly distributed on the fiber surface, but the content of Ba was different, and the characteristic peak of Ba was higher than that in Ba/CAF-8.0/B. This is due to the high concentration of Ba^{2+} in combination B, which leads to the adhesion of more solidified material on the fiber surface, and it is also proved by SEM images. The characteristic peak of Ba in Ba/CAF-8.0/C is slightly lower, which is related to the low concentration of Ba^{2+} in the C combination. The content of Ba elements in Ba/CAF-8.0/A, Ba/CAF-8.0/B and Ba/CAF-8.0/C is uniformly distributed, which indicates that the pre-crosslinking process realizes the full combination of Ba^{2+} and CA sulfate groups [20].

Ba/CAF-8.0/A, Ba/CAF-8.0/B and Ba/CAF-8.0/C showed similar FTIR spectra (Fig. 6). The peaks at 3400 cm^{-1} and 2900 cm^{-1} are the stretching vibration of hydroxyl group and the asymmetric stretching vibration of C-H group, respectively. The characteristic peak near 1070 cm^{-1} is related to the C3-O-C6 bridge in the dehydration D-galactose residue (DA2S) of CA molecule, and the peak at 1020 cm^{-1} indicates the presence of C-O bond in the DA2S unit. The peaks of 840 cm^{-1} attributed to the sulfate group on D-galactose-4-sulfate (G4S) C4 and the presence of a peak near 805 cm^{-1} indicates the presence of a sulfate group on DA2S unit C2. The characteristic peak at 1420 cm^{-1} is attributed to the methylene associated with oxygen, and the absorption peak of Ba/CAF-8.0/A here is significantly enhanced due to the dehydration of ethanol in combination A. The characteristic peak around 1220 cm^{-1} is the stretching vibration of S=O in the sulfate group of CA molecule, and the characteristic peaks of Ba/CAF-8.0/B and Ba/CAF-8.0/C become wider here, which may be caused by the sufficient combination of Ba^{2+} with the sulfate group in CA molecule.

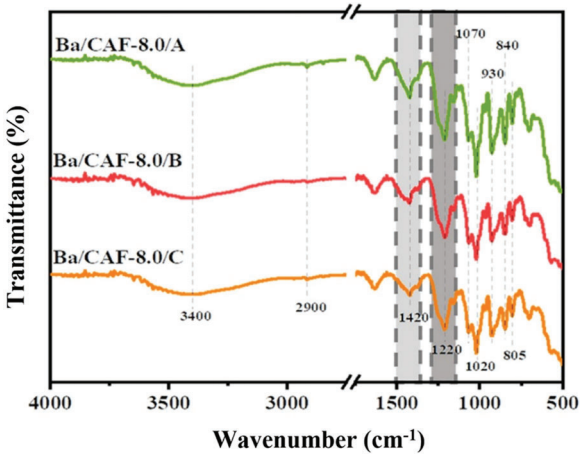

Figure 6: FTIR spectra of Ba/CAF-8.0/A, Ba/CAF-8.0/B and Ba/CAF-8.0/C

The strength of fiber is a decisive factor limiting its application. How to prepare high-strength CAF has become a research hotspot in this field [21]. The breaking strength, breaking elongation and fracture time of the fibers are shown in Fig. 7, in which Ba/CAF-8.0/A has the highest value of breaking elongation, up to

12.89%; the breaking strength is slightly lower as 1.40 cN/dtex; and the fracture time is the longest as to 7.73 s. Ba/CAF-8.0/C has the highest breaking strength, up to 1.61 cN/dtex, the breaking elongation is slightly weaker (12.26%), and the fracture time is 7.59 s. The mechanical properties of Ba/CAF-8.0/B are not superior, the breaking elongation is 8.35%, the breaking strength is 1.27 cN/dtex, and the fracture time is 5.26 s.

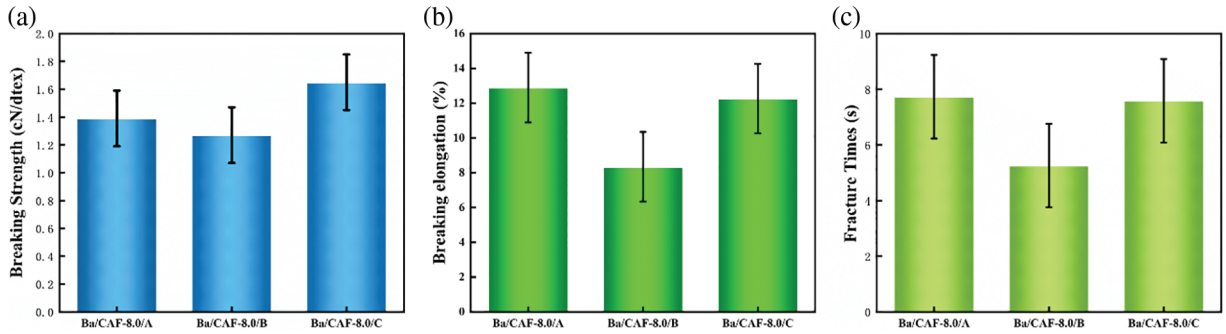

Figure 7: The mechanical properties of Ba/CAF-8.0/A, Ba/CAF-8.0/B and Ba/CAF-8.0/C (a. Breaking strength; b. Breaking elongation; c. Fracture time)

The same concentration of spinning solution gets different mechanical properties after wet-spinning through the coagulation and stretch baths with combination A, B and C [22]. In combination A, the regular pre-crosslinked structure in the spinning solution was not destroyed by ethanol in coagulation and stretch baths, which help Ba/CAF-8.0/A obtain a high degree of regularity. At the same time, the hydrogen bond formed in the fiber formation process also improved the mechanical properties of the fiber [12,23]. However, Ba^{2+} in combination B and C has a complex effect on the mechanical properties of the fibers: the pre-crosslinked structure formed in the spinning solution will be affected by Ba^{2+} in coagulation and stretch baths, and the higher the concentration of Ba^{2+}, the more obvious the damage effect on the original pre-crosslinked structure. This has a weakening effect on the mechanical properties of the fibers.

On the other hand, the ionic bond formed by the combination of Ba^{2+} with the sulfate group in CA molecule can improve the mechanical strength of the fiber, and the presence of Ba^{2+} in coagulation and stretch baths can enhance the mechanical properties of the fiber. Therefore, the mechanical properties of Ba/CAF-8.0/B and Ba/CAF-8.0/C are comprehensively affected by the above two effects. Different concentrations of Ba^{2+} have different solidify effects in the fiber formation process. The high concentration of Ba^{2+} in combination B may rapidly combine with the sulfate group in CA molecules, resulting in the rapid formation of a dense structural layer on the fiber surface, uneven internal and external structure of the fiber and reduced flexibility. Some Ba/CAF-8.0/B surface defects occur during fiber formation due to high concentration of Ba^{2+} aggregation, thus affecting the mechanical properties of the fibers, which is also verified by the specific analysis of fiber morphology.

However, due to the low concentration of Ba^{2+} in combination C, the binding process of Ba^{2+} and CA molecules is relatively mild, and Ba^{2+} can enter the interior of the fiber in a gradual permeable way, so that the internal and external bonding degree of the fiber is uniform. At the same time, low concentration of Ba^{2+} has little effect on the original pre-crosslinked structure in the spinning solution, and the regular arrangement of CA molecules is preserved in Ba/CAF-8.0/C to a certain extent. Therefore, the mechanical properties of the fibers are improved under the joint action of the two.

In sum, Ba/CAF-8.0/C exhibits the best mechanical properties under the action of uniformly bonded ionic bond and partially preserved pre-crosslinked structure, and Ba/CAF-8.0/A exhibits the second mechanical properties under the action of hydrogen bond and maximally preserved pre-crosslinked structure. However, the mechanical properties of Ba/CAF-8.0/B are the worst while the pre-crosslinked structure is destroyed and the degree of fiber internal and external bonding is uneven.

The water absorption performance of fiber is one of the important factors affecting the comfort [24]. The water absorption performance of Ba/CAF-8.0/A, Ba/CAF-8.0/B and Ba/CAF-8.0/C were tested in deionized water and normal saline, respectively. The results were shown in Fig. 8. Ba/CAF-8.0/A, Ba/CAF-8.0/B and Ba/CAF-8.0/C all showed good hydrophilicity, which was related to the high content of hydroxyl groups in the molecular structure of CA. Among them, Ba/CAF-8.0/A had the highest water absorption, which is 727.1% in deionized water and 684.5% in normal saline. Due to the obvious swelling during the process of water absorption, some fibers adhered and clustered. Ba/CAF-8.0/B had the lowest water absorption, which is 478.4% in deionized water and 450.6% in normal saline, which was related to the higher concentration of Ba^{2+} in coagulation bath. The combination of Ba^{2+} with sulfate group makes Ba/CAF-8.0/B compact and dense, which played a role in reducing water absorption and maintaining good shape. The water absorption of Ba/CAF-8.0/C in deionized water and normal saline was 649.2% and 574.3%, respectively, slightly higher than that of Ba/CAF-8.0/B. It was mainly due to the decrease of Ba^{2+} concentration in coagulation bath.

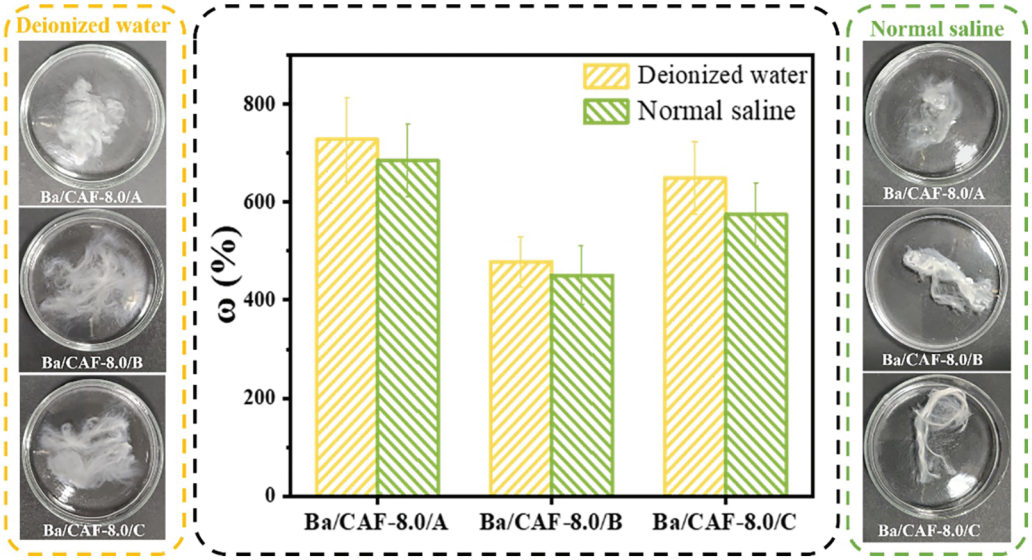

Figure 8: Water absorption of Ba/CAF-8.0/A, Ba/CAF-8.0/B and Ba/CAF-8.0/C

However, compared with the dehydration of ethanol, the ionic bond formed by Ba^{2+} combined with sulfate group made the structure of Ba/CAF-8.0/C more compact, and the water absorption of Ba/CAF-8.0/C was significantly lower than that of Ba/CAF-8.0/A.

The flame retardancy properties of Ba/CAF-8.0/A, Ba/CAF-8.0/B and Ba/CAF-8.0/C were characterized by LOI test, and the experimental data were shown in Table 1 and the combustion of Ba/CAF-8.0/A, Ba/CAF-8.0/B and Ba/CAF-8.0/C in LOI test are shown in Fig. 9. During the test process, the gas flow is adjusted according to the order of oxygen concentration from low to high, and the oxygen concentration is the LOI value when the sample is self-extinguished within 30 s after ignition [25,26]. Ba/CAF-8.0/A fails to ignite at an oxygen concentration of 29% (Fig. $9a_2$); Self-extinguishing

after ignition at 30% oxygen concentration (Fig. 9a$_4$); When the oxygen concentration is 31%, the smolder state of red heat is maintained for more than 30 s (Fig. 9 a$_6$), so the LOI test result of Ba/CAF-8.0/A is 30. Under the same test conditions, the LOI value of Ba/CAF-8.0/B is 33 and the LOI value of Ba/CAF-8.0/C is 32.

Table 1: Data of Ba/CAF-8.0/A, Ba/CAF-8.0/B and Ba/CAF-8.0/C in LOI test

Sample	Oxygen concentration (%)	Oxygen flow (L/min)	Nitrogen flow (L/min)	LOI (%)
Ba/CAF-8.0/A	29.0	3.31	8.09	**30**
	30.0	3.42	7.98	
	31.0	3.53	7.87	
Ba/CAF-8.0/B	32.0	3.65	7.75	**33**
	33.0	3.76	7.64	
	34.0	3.88	7.52	
Ba/CAF-8.0/C	31.0	3.53	7.87	**32**
	32.0	3.65	7.75	
	33.0	3.76	7.64	

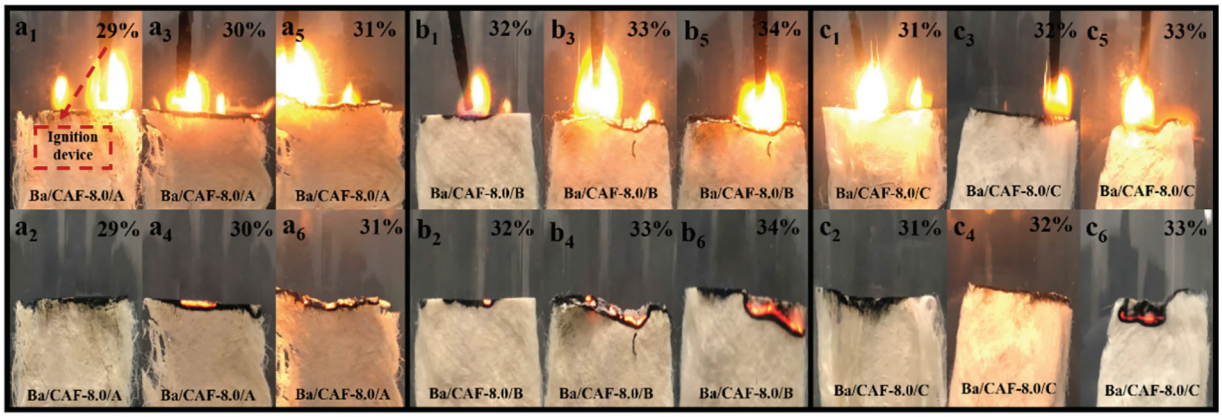

Figure 9: Combustion of Ba/CAF-8.0/A, Ba/CAF-8.0/B and Ba/CAF-8.0/C in LOI test. a$_1$, a$_3$, a$_5$, b$_1$, b$_3$, b$_5$, c$_1$, c$_3$, c$_5$ light Ba/CAF-8.0s with a burning igniter. a$_2$, a$_4$, a$_6$, b$_2$, b$_4$, b$_6$, c$_2$, c$_4$, c$_6$ remove Ba/CAF-8.0s from light

The flame retardancy properties of carrageenan fibers prepared by different coagulating bath and stretching bath combination are different. The LOI value of Ba/CAF-8.0/A is the smallest among the three, and the LOI values of Ba/CAF-8.0/B and Ba/CAF-8.0/C are not significantly different, which is consistent with the flame retardant theory of metal ions: in the combustion process, Ba^{2+} combines with sulfonyls residues to form $BaSO_4$, which plays a role in blocking the exchange of heat and gas, thus improving the flame retardant property of the fibers. Ba/CAF-8.0/B formed a dense structure of $BaSO_4$ during combustion and has a better flame retardancy effect, so the LOI value of Ba/CAF-8.0/B is the largest.

3.3 Fiber Formation Process of Ba/CAF

All characterization of the spinning stock and fibers confirmed the possible fiber formation mechanism of Ba/CAF (Fig. 10). In the process of pre-crosslinking, the sulfate group in CA molecule is combined with

Ba^{2+} to a certain extent, and the molecular chain of CA molecule is connected by the ionic bond formed with Ba^{2+}, and the conformation of the molecular chain is changed from random linear group to regular order [27–29].

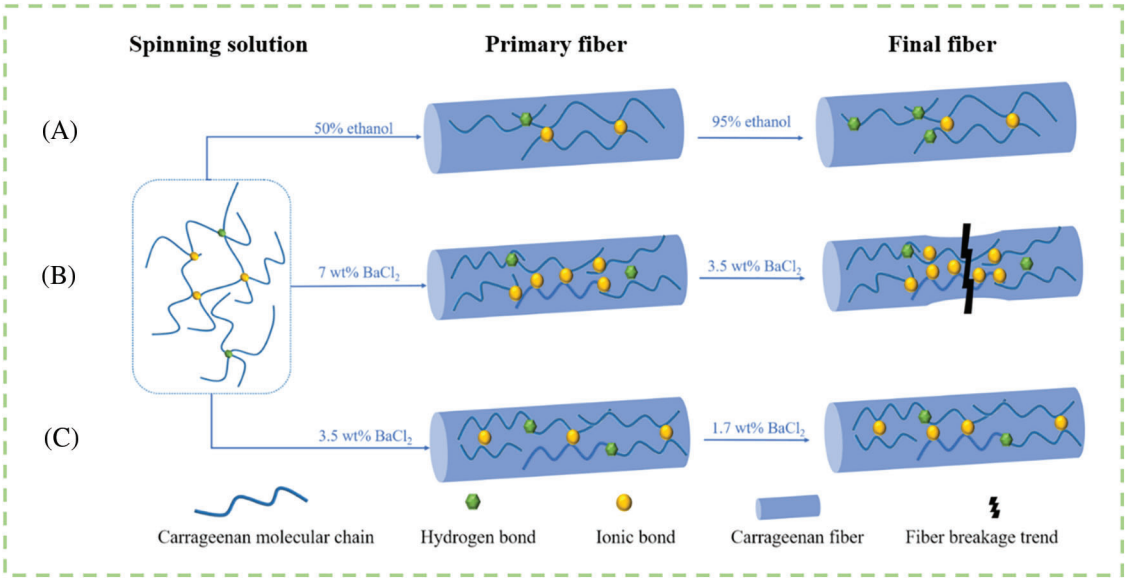

Figure 10: Schematic diagram of Ba/CAF-8.0 formation process of combination A, B and C of coagulation and stretch baths

When the spinning solution is dehydrated by ethanol solution, the CA molecular chains gradually get closer in the process of water loss, and the pre-crosslinked structure formed in the spinning solution basically remains unchanged [30]. The increase in chain density promotes the formation of hydrogen bonds, and the mechanical properties of Ba/CAF-8.0/A are therefore enhanced. However, since the source of Ba^{2+} is only the small amount of $BaCl_2$ added during pre-crosslinking, the flame retardancy of Ba/CAF-8.0/A is slightly worse than that of Ba/CAF-8.0/B and Ba/CAF-8.0/C.

When the spinning solution is solidified into fiber in $BaCl_2$ solution, the CA molecular chains are connected by ionic bonds formed with Ba^{2+}, which affects the pre-crosslinked structure formed in the spinning solution, and the higher the concentration of Ba^{2+}, the more obvious the destructive effect.

More Ba^{2+} is involved in the fiber formation process in combination B, so Ba/CAF-8.0/B can maintain a good fiber shape in the water absorption test and show better flame retardancy performance in the LOI test. However, due to the formation of some ionic bonds in the pre-crosslinking process, too high concentration of Ba^{2+} in the coagulation bath will lead to uneven bonding degree. SEM images also show that there are defects on Ba/CAF-8.0/B surface, and the mechanical strength of Ba/CAF-8.0/B is reduced due to uneven bonding, and even fracture tendency occurs during stretching. Similarly, under the action of Ba^{2+}, the water absorption and flame retardancy of Ba/CAF-8.0/C have shown good experimental results [31]. The difference is that due to the appropriate concentration of Ba^{2+} in combination C, the Ba/CAF-8.0/C ionic bond is uniformly formed during the fiber formation process, and the regular arrangement of CA molecules in the pre-crosslinked structure is retained to a certain extent. The resulting stable three-dimensional network structure makes the interior of the fiber dense and compact [32], thus optimizing the performance of Ba/CAF-8.0/C.

4 Conclusion

In this study, an extremely small amount of Ba^{2+} was introduced into the spinning solution to achieve the ordered distribution of CA molecular chains in the spinning solution by pre-crosslinking. The results showed that when the mass fraction of CA was 8.0 wt%, the degree of Ba^{2+} pre-crosslinking was optimal. PLM tests show that Ba^{2+} can induce CA molecular chain to form birefringence. MRV and DLS tests show that Ba/CA-8.0 has a viscosity of 32193 mPa·s and an average particle size of 1475 nm.

In addition, the combination of coagulation bath and stretch bath suitable for wet spinning by Ba^{2+} pre-crosslinking method was screened, and Ba/CAF/A, Ba/CAF/B and Ba/CAF/C with different CA mass fractions were prepared by ethanol solution, high concentration $BaCl_2$ solution and low concentration $BaCl_2$ solution. From the perspective of production safety, fiber properties and spinning cost, the combination C, that is, low concentration $BaCl_2$ solution, is the best choice. The test results of SEM, EDS, and FTIR show that Ba^{2+} bonds uniformly during the fiber formation process, and Ba/CAF-8.0/C has better mechanical properties. The breaking strength is 1.61 cN/dtex; The flame retardancy showed good experimental results, the LOI value reached 32, and it showed good hydrophilicity in deionized water and normal saline, the water absorption was 649.2% and 574.3%, respectively.

The preparation time of spinning solution is shortened by 1.5 h through Ba^{2+} pre-crosslinking, and the preparation process is simpler and more efficient. The new process provides sufficient contact time between metal ions and CA molecules in the spinning solution, and guarantees the construction of pre-crosslinked structures. The performance of CAF prepared by ion pre-crosslinking method has been significantly improved. At the same time, the selection of low concentration salt solution can avoid the difference in the performance of the same batch of fiber due to the rapid change of concentration. This division provides a new idea for the optimization of metal ion pre-crosslinked wet spinning process.

Acknowledgement: The authors thank the Program of the National Natural Science Foundation of China, Natural Science Foundation of Shandong Province, State Key Laboratory of Bio-Fibers and Eco-Textiles of Qingdao University, and the Program for Changjiang Scholars and Innovative Research Team in University of Ministry of Education of China for their financial support.

Funding Statement: This work was financially supported by the Program of the National Natural Science Foundation of China (52173037), Natural Science Foundation of Shandong Province (ZR2020ME061), State Key Laboratory of Bio-Fibers and Eco-Textiles of Qingdao University (ZFT201810, ZKT17, TSKT202107), and the Program for Changjiang Scholars and Innovative Research Team in University of Ministry of Education of China (IRT14R30).

Author Contributions: The authors confirm contribution to the paper as follows: study conception and design: Zhixin Xue, Liting Jia, Xiao Han; data collection: Cuixia Qiao, Yanzhi Xia, Gang Zhao, Zhixin Xue; analysis and interpretation of results: Zhixin Xue, Liting Jia, Xiao Han, Cuixia Qiao, Yanzhi Xia; draft manuscript preparation: Zhixin Xue, Liting Jia, Xiao Han. All authors reviewed the results and approved the final version of the manuscript.

Availability of Data and Materials: Data available on request from the authors. The data that support the findings of this study are available from the corresponding author, (Xue), upon reasonable request.

Conflicts of Interest: The authors declare that they have no conflicts of interest to report regarding the present study.

References

1. Ghanbarzadeh, M., Golmoradizadeh, A., Homaei, A. (2018). Carrageenans and carrageenases: Versatile polysaccharides and promising marine enzymes. *Phytochemistry Reviews, 17(3),* 535–571.

2. Zia, K. M., Tabasum, S., Nasif, M., Sultan, N., Aslam, N. et al. (2017). A review on synthesis, properties and applications of natural polymer based carrageenan blends and composites. *International Journal of Biological Macromolecules, 96,* 282–301.
3. Jiang, C., Jiang, H., Zhang, T., Lu, Z., Mao, X. (2022). Enzymatic verification and comparative analysis of carrageenan metabolism pathways in marine bacterium flavobacterium algicola. *Applied and Environmental Microbiology, 88(7),* e0025622.
4. Prechoux, A., Genicot, S., Rogniaux, H., Helbert, W. (2013). Controlling carrageenan structure using a novel formylglycine-dependent sulfatase, an endo-4S-iota-carrageenan sulfatase. *Marine Biotechnology, 15(3),* 265–274.
5. Abad, L. V., Aranilla, C. T., Relleve, L. S., Dela Rosa, A. M. (2014). Emerging applications of radiation-modified carrageenans. *Nuclear Instruments & Methods in Physics Research Section B-Beam Interactions with Materials and Atoms, 336,* 167–172.
6. Praseptiangga, D., Widyaastuti, D., Panatarani, C., Joni, I. M. (2021). Development and characterization of semi-refined iota carrageenan/SiO_2-ZnO bionanocomposite film with the addition of cassava starch for application on minced chicken meat packaging. *Foods, 10(11),* 2776.
7. Dong, M., Xue, Z. X., Wang, L. L., Xia, Y. Z. (2018). NaOH induced the complete dissolution of iota-carrageenan and the corresponding mechanism. *Polymer, 151,* 334–339.
8. Li, G., Zhang, G., Sun, R., Wong, C. P. (2017). Mechanical strengthened alginate/polyacrylamide hydrogel crosslinked by barium and ferric dual ions. *Journal of Materials Science, 52(14),* 8538–8545.
9. Pan, Y., Wang, W., Liu, L., Ge, H., Song, L. et al. (2017). Influences of metal ions crosslinked alginate based coatings on thermal stability and fire resistance of cotton fabrics. *Carbohydrate Polymers, 170,* 133–139.
10. Bajpai, S. K., Saxena, S. K., Sharma, S. (2006). Swelling behavior of barium ions-crosslinked bipolymeric sodium alginate-carboxymethyl guar gum blend beads. *Reactive & Functional Polymers, 66(6),* 659–666.
11. Aneem, T. H., Wong, S. Y., Afrin, H., Nurunnabi, M., Li, X. et al. (2021). Investigation of coagulation process of wet-spun sodium alginate polymannuronate fibers with varied functionality using organic coagulants and cross-linkers. *Materials Today Chemistry, 22,* 100580.
12. Dong, M., Zhang, K., Wang, L., Han, J., Wang, Y. et al. (2020). High-strength carrageenan fibers with compactly packed chain structure induced by combination of Ba^{2+} and ethanol. *Carbohydrate Polymers, 236,* 116057.
13. Lu, Z., Lin, Z., Wang, Q., Song, P. (2023). Short communication metal-organic framework-derived Au-In_2O_3 nested hierarchical structures for ethanol detection at room temperature. *Inorganic Chemistry Communications, 155,* 111121.
14. Lytle, D. A., Wahman, D. G., Schock, M. R., Nadagouda, M. N., Harmon, S. et al. (2019). Georgeite: A rare copper mineral with important drinking water implications. *Chemical Engineering Journal, 355,* 1–10.
15. Wang, Z., Chen, X., Song, X., Zeng, Y., Li, P. et al. (2022). Domain memory effect in the organic ferroics. *Nature Communications, 13(1),* 2379.
16. Wang, Y., Tong, Y., Zhang, B., Su, H., Xu, L. (2018). Formation of surface morphology in polyacrylonitrile (PAN) fibers during wet-spinning. *Journal of Engineered Fibers and Fabrics, 13(2),* 52–57.
17. Le Troedec, M., Peyratout, C. S., Smith, A., Chotard, T. (2009). Influence of various chemical treatments on the interactions between hemp fibres and a lime matrix. *Journal of the European Ceramic Society, 29(10),* 1861–1868.
18. Essabir, H., Bensalah, M. O., Rodrigue, D., Bouhfid, R., Qaiss, A. (2016). Structural, mechanical and thermal properties of bio-based hybrid composites from waste coir residues: Fibers and shell particles. *Mechanics of Materials, 93,* 134–144.
19. Talik, P., Moskal, P., Proniewicz, L. M., Weselucha-Birczynska, A. (2020). The raman spectroscopy approach to the study of water-polymer interactions in hydrated hydroxypropyl cellulose (HPC). *Journal of Molecular Structure, 1210(15),* 128062.
20. Fu, M., Wu, Y., Zhang, Q., Xue, Z., Geng, C. et al. (2021). Study on the mechanical and flame retardant properties of a novel carrageenan fiber-CAF-K,Al. *European Polymer Journal, 105(5),* 11408.
21. Ma, L., Zhao, Y., Wang, Y., Shang, L., Hua, J. (2017). QTLs analysis and validation for fiber quality traits using maternal backcross population in upland cotton. *Frontiers in Plant Science, 8,* 2168.

22. Hu, J., Li, R., Zhu, S., Zhang, G., Zhu, P. (2021). Facile preparation and performance study of antibacterial regenerated cellulose carbamate fiber based on N-halamine. *Cellulose, 28(8),* 4991–5003.
23. Zhao, X., Xia, Y., Zhang, X., Lin, X., Wang, L. (2019). Design of mechanically strong and tough alginate hydrogels based on a soft-brittle transition. *International Journal of Biological Macromolecules, 139,* 850–857.
24. Kumar, S., Saha, A. (2022). Utilization of coconut shell biomass residue to develop sustainable biocomposites and characterize the physical, mechanical, thermal, and water absorption properties. *Biomass Conversion and Biorefinery, 22(4),* 2190–6823.
25. Loganathan, T. M., Hameed Sultan, M. T., Ahsan, Q., Jawaid, M., Naveen, J. et al. (2021). Effect of *cyrtostachys renda* fiber loading on the mechanical, morphology, and flammability properties of multi-walled carbon nanotubes/phenolic bio-composites. *Nanomaterials, 11(11),* 3049.
26. Liu, Z., Li, J., Zhao, X., Li, Z., Li, Q. (2018). Surface coating for flame retardancy and pyrolysis behavior of polyester fabric based on calcium alginate nanocomposites. *Nanomaterials, 8(11),* 875.
27. Mao, Y., Zhou, J., Cai, J., Zhang, L. (2006). Effects of coagulants on porous structure of membranes prepared from cellulose in NaOH/urea aqueous solution. *Journal of Membrane Science, 279(1–2),* 246–255.
28. Medinatorres, L., Britodelafuente, E., Gomezaldapa, C., Aragonpina, A., Torovazquez, J. (2006). Structural characteristics of gels formed by mixtures of carrageenan and mucilage gum from Opuntia ficus indica. *Carbohydrate Polymers, 63(3),* 299–309.
29. Zheng, T., Abadi, P. P. S. S., Seo, J., Cha, B. H., Miccoli, B. et al. (2019). Biocompatible carbon nanotube-based hybrid microfiber for implantable electrochemical actuator and flexible electronic applications. *ACS Applied Materials & Interfaces, 11(23),* 20615–20627.
30. Zhang, W., Lin, L., Guo, J., Wu, M., Park, S. et al. (2022). Design strategy for vulcanization accelerator of diphenylguanidine/cyclodextrin inclusion complex for natural rubber latex foam with enhancing performance. *Research, 2022(9),* 9814638.
31. Zhang, X., Yan, H., Xu, C., Dong, X., Wang, Y. et al. (2023). Skin-like cryogel electronics from suppressed-freezing tuned polymer amorphization. *Nature Communications, 14(1),* 5010.
32. Zhang, L., Wang, X., Qu, W., Zhang, A., Wahia, H. et al. (2022). Evaluation of dual-frequency multi-angle ultrasound on physicochemical properties of tofu gel and its finished product by TOPSIS-entropy weight method. *Ultrasonics Sonochemistry, 90,* 106196.